Terahertz Sensors Using Surface Waves in Periodic Metallic Structures

by

Hadi Amarloo

A thesis
presented to the University of Waterloo
in fulfillment of the
thesis requirement for the degree of
Master of Applied Science
in
Electrical and Computer Engineering

Waterloo, Ontario, Canada, 2013

AUTHOR'S DECLARATION

I hereby declare that I am the sole author of this thesis. This is a true copy of the thesis, including any required final revisions, as accepted by my examiners.

I understand that my thesis may be made electronically available to the public.

Abstract

Terahertz range of frequency has found a fast growing number of applications in material characterization and sensing, imaging and extreme bandwidth communication. Different structures have been proposed for sensing at these frequencies. Surface plasmon waves have successfully been applied to ultra-high precision sensing at optical frequencies, because of their strong field confinement and enhancement. These waves are not as confined in THz due to metal properties over this range of frequencies. However, it has been shown that surface waves on properly designed periodic metallic structure have behavior very similar to plasmonic waves in optical range. These surface wave modes are called surface plasmon-like waves.

Here we consider several periodic metallic structures, which support these surface plasmon-like modes, for THz sensing applications. The first one is a two dimensional array of metallic rods which is excited by prism. Many existing plasmonic sensing configurations use prism for plasmonic wave excitation. However, prism is too bulky for integration. Interests in integrated surface plasmonic devices at optical frequencies have been growing recently. As compared with free space configuration, integrated structures have distinct advantages such as small size and multi-channel sensing capabilities. An integrated sensing configuration using plasmonic-like wave is proposed. The new configuration uses a metallic grating that acts as a THz waveguide with a stop-band with a sharp transition edge. Excitation of such metallic grating waveguide through a dielectric waveguide will be described and analyzed. Moreover, it will be shown that the frequency of the transition edge between pass-band and stop-band is highly sensitive to the refractive index of the surrounding medium, and therefore it can be used for dielectric sensing. The excitation requirements of the proposed sensor and its sensitivity will be presented.

Acknowledgements

I would like to thank god for blessing me. I would like to thank my parents for their unconditional love and support.

Special thanks to my supervisor Professor Safavi-Naeini for his support, kindness and encouragement during my MSc. I am very grateful of him for his insightful discussions and comments.

I would like to thank Dr. Rohani, Dr. Neshat and Dr. Arbabi for their collaborating and helpful discussions. I would like to thank Dr. Khorasaninejad for his efforts and helps during fabrication part of this project.

Dedication

To my parent for their endless love

Table of Contents

List of Figures

List of Tables

Chapter 1
Introduction

1.1 Motivation

THz Technology and its Applications:

Terahertz range of frequency, which is in between infrared and microwave frequency, is usually referred as frequencies from 300 GHz to 3 THz which corresponds to the wavelengths from 100 μm to 1000 μm. THz range is an undeveloped region compared to other parts of the electromagnetic spectrum. Figure 1.1 shows electromagnetic spectrum and THz gap.

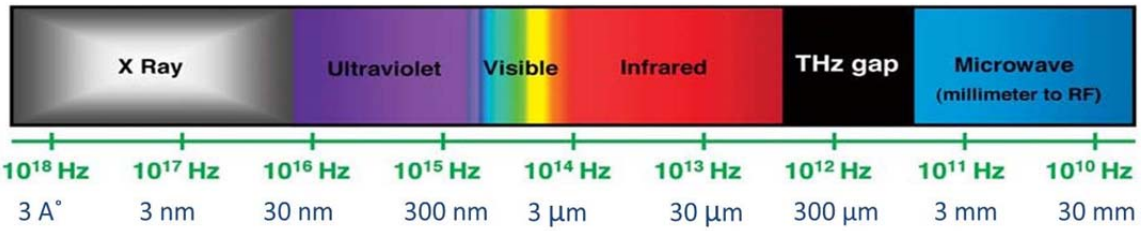

Figure 1.1 Electromagnetic Spectrum

This range of frequency has found a fast growing number of applications like: information and communications technology (ICT), biology and medical sciences, non-destructive evaluation, homeland security, quality control of food and agricultural products, global environmental monitoring and ultrafast computing [1]. This is mainly due to the fact that many important materials have specific signatures over these frequencies. As an example, water, a polar liquid, is highly absorptive at THz range. Figure 1.2 shows water molecule rotational and vibrational resonances and on the right, shows absorption spectrum for 10 cm path at atmospheric pressure in the Spectral range 0.3-6 THz on the left [2].

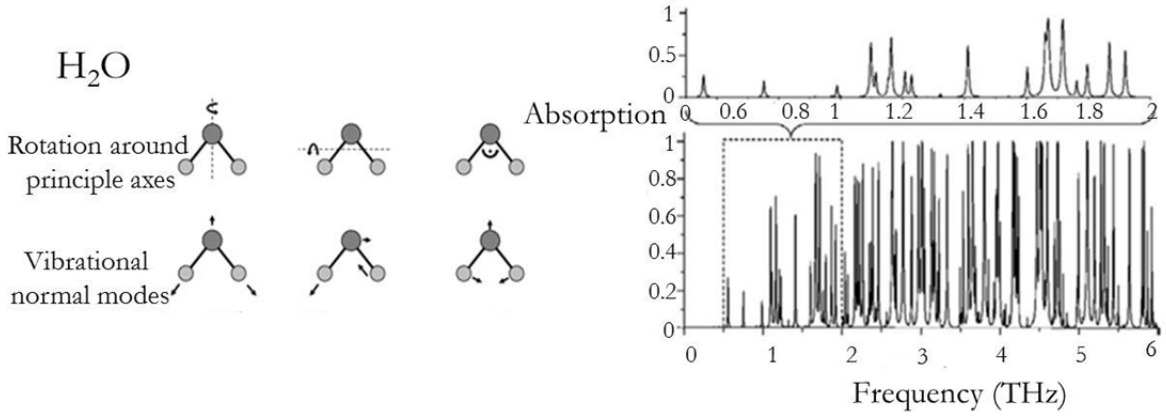

Figure 1.2 left: Water molecule rotational and vibrational resonances, right: absorption spectrum of water for 10-cm path at atmospheric pressure in the spectral range 0.3-6 THz [2]

By using of water features in THz range, hydrated substances are easily differentiated from dried ones. In a biological system, small changes in water content could indicate crucial defects emerging in the region. This makes high sensitivity of THz radiation to water useful for medical applications.

Nonpolar and nonmetallic materials, dielectrics such as paper, plastic, clothes, wood and ceramics that are usually opaque at optical wavelengths, are transparent to THz radiation. Since common packaging materials are dielectric, THz imaging is applied to nondestructive testing to inspect sealed packages.

An intriguing application of THz spectroscopy of biomolecules is to directly probe the binding states of genetic material without using fluorescent labels. Fig. 1.3 shows the real and imaginary parts of refractive index of hybridized and denatured DNA films [2].

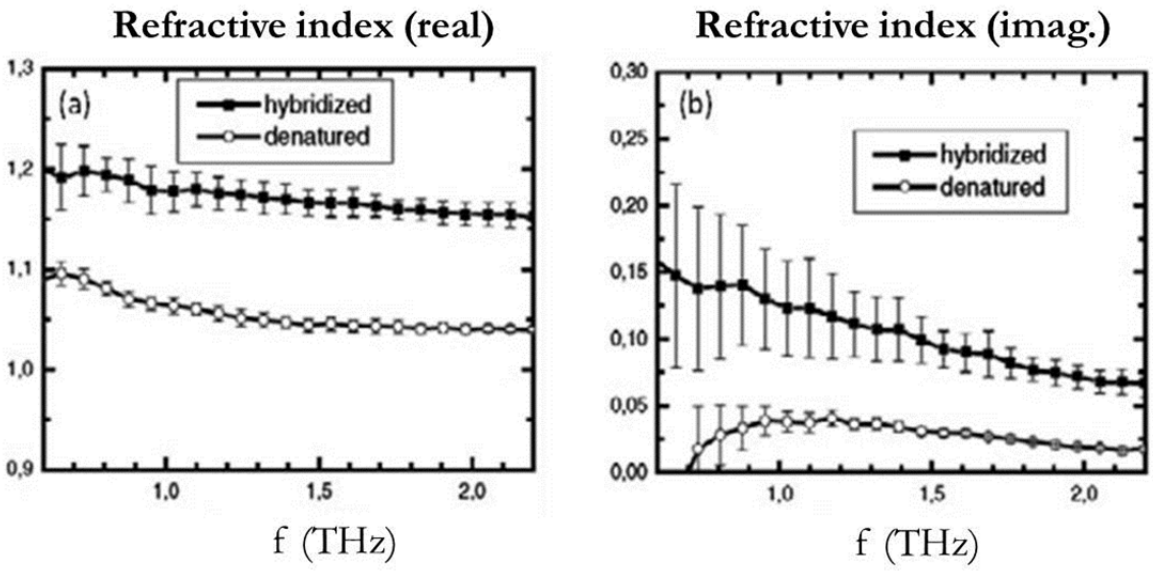

Figure 1.3 (a) Real and (b) imaginary parts of the refractive index of hybridized and denatured DNA films [2]

Both real and imaginary parts of refractive index of denatured DNA are considerably smaller than those of hybridized DNA, meaning that the interaction of THz radiation with denatured DNA is much weaker than that with hybridized DNA. It can be accounted for by the fact that double-stranded DNA structure surely has a higher vibrational mode density than single-stranded in the THz region. Regardless of the microscopic nature causing the difference, the ultimate outcome of this experimental observation is that THz spectroscopy is applicable to label-free identification of DNA binding states.

THz Sensing Using Plasmonic Waves

One of the main important applications of THz frequencies is biomedical sensing and imaging. The wavelength at THz range of frequency is much longer than the wavelength at optical frequencies. So the samples which are electrically large for optical frequencies will be sub-wavelength at THz range. So THz sensors which can sense sub-wavelength sample features are particularly desirable. In the optical range of frequency it is well established that surface plasmon waves can be used for highly sensitive measurements because of high confinement of fields. In THz range, surface plasmon waves on flat metals are not confined

and therefore cannot be used for sub-wavelength sensing. But it has been shown that periodic metallic structures support surface waves at THz frequencies which has similar properties as plasmonic waves in optical range.

Use of surface waves on periodic metallic structures, as a replacement of plasmonic wave for THz range, has found vast attention in many groups [3-7]. Surface wave on periodic metallic structures is usually called palsmonic-like waves, because it has properties similar to plasmonic waves at optical frequencies. The main property of plasmonic and plasmonic-like waves is high confinement of the fields which makes them useful for sensing of sub-wavelength sample features. In this thesis we use the properties of these waves to have sensitive sensors in THz range.

1.2 Thesis Overview

The next chapter is an introduction to plasmonics and plasmonic-like waves. Starting with plasmonic waves in optical regime and metal properties at that range of frequency, features of surface plasmon waves are presented. Then plasmonic waves and plasmonic-like waves at lower frequency, including THz range, are discussed. The capability of periodic metallic structures to have plasmonic-like waves in THz range is presented. As a simple example, one dimensional metallic grating and then a two dimensional array of holes in metal plate are discussed to show the similarity of surface waves at low frequency to the plasmonic waves at optical frequencies.

In [8] a two dimensional photonic crystal structure is presented. Chapter 3 will take a look at this structure and continue some more analysis on its performance. In this configuration, prism is used for the excitation of surface waves. The device operation is discussed and simulation results from HFSS simulations are presented. The structures which work based on the plasmonic or plasmonic-like waves are sensitive to the fabrication tolerance because of high confinement of surface waves. Fabrication errors affect the performance of devise.

Simulations which show these effects are presented to find out the accuracy which is needed in fabrication process.

For many advantages, always integrated elements are preferred. In recent years some groups have presented structures which use plasmonic waves for sensing in integrated configurations. In chapter 4, a new integrated scheme for THz sensing is presented. The presented structure use metallic grating which support surface waves as the sensing part. The device performance is investigated using COMSOL simulations and the results are discussed.

Thesis will be finished by conclusions in Chapter 5and References.

Chapter 2

THz Plasmonics

2.1 Plasmonics

Surface plasmon polaritons are collective oscillation of electrons coupled to electromagnetic field that occur at an interface between a conductor and a dielectric [9]. Metals show large imaginary and negative real permittivity at frequencies up to THz range, so can be assumed as perfect electric conductor (PEC). But for optical frequencies, the free electrons of metal cannot respond to the electric filed spontaneously. Using a simple second order differential equation of motion for an electron in the plasma sea, the conductance and consequently the complex permittivity for metals can be found as [9]:

$$\varepsilon_r(\omega) = 1 - \frac{\omega_p}{\omega(\omega - j\omega_t)} \tag{2.1}$$

In which, ω_t is collision frequency and ω_p is plasma frequency of free electron gas. This model is called the Drude model. For large frequencies close to ω_p, $\omega \gg \omega_t$, then $\varepsilon_r(\omega)$is predominantly real, and:

$$\varepsilon_r(\omega) = 1 - \frac{{\omega_p}^2}{\omega^2} \tag{2.2}$$

As equation (2.2) shows, the permittivity of metals is negative at frequencies smaller than plasma frequency. As will be discussed in the next section, this negative permittivity of metals leads to existence of surface waves which propagates along a metal dielectric interface and are referred to as surface plasmon polaritons.

2.1.1 Surface Plasmon on a Flat Metal-Dielectric Interface

To find properties of propagating surface plasmon waves, plasmonic wave in a flat dielectric-metal interface can be considered as shown in Fig. 2.1.

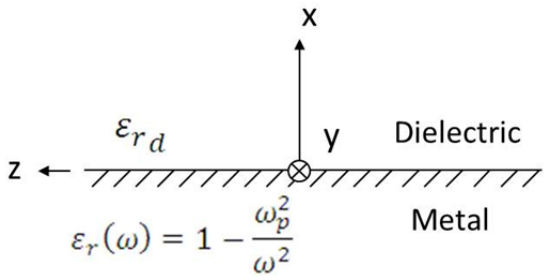

Figure 2.1 Flat interfaces of metal and a dielectric

The metal part is modeled with Drude model permittivity which was shown in previous part. Considering TE_z mode first, we are looking for TE modes which are propagating in *z* direction and are bounded to the interface. So:

$$H_y = E_x = E_z = 0 \tag{2.3}$$

$$H_x = Ce^{Kx} + De^{-Kx} \tag{2.4}$$

Parameters for dielectric region will be shown by *d* and for metal region by *m*. Looking at equation (2.4), to have finite fields, if we assume $Re\ K_d > 0$, then C_d should be zero, and if $Re\ K_m > 0$, then D_m should be zero. To find the constants, continuity of transverse component, H_z and E_y, at the interface should be applied.

$$K = \sqrt{k_z^2 - \omega^2 \varepsilon_r \mu_r / c_0^2}, \quad \mathrm{Re}\, K > 0 \tag{2.5}$$

$$\left.\begin{aligned} C_m \mu_{r_m} &= D_d \mu_{r_d} \\ C_m K_m &= -D_d K_d \end{aligned}\right\} \Rightarrow \frac{K_m}{\mu_{r_m}} + \frac{K_d}{\mu_{r_d}} = 0 \tag{2.6}$$

Since real part of K_m and K_d are positive, this equation cannot be satisfied. So this structure does not support TE modes.

TM modes can be analyzed in the same way as discussed for TE case.

$$E_y = H_x = H_z = 0 \tag{2.7}$$

$$E_x = Ae^{Kx} + Be^{-Kx} \tag{2.8}$$

$$\left.\begin{aligned} A_m \varepsilon_{r_m} &= B_d \varepsilon_{r_d} \\ A_m K_m &= -B_d K_d \end{aligned}\right\} \Rightarrow \frac{K_m}{\varepsilon_{r_m}} + \frac{K_d}{\varepsilon_{r_d}} = 0 \tag{2.9}$$

Because ε_{r_m} is negative for the frequencies below ω_p, so this relation is possible and so the structure supports TM modes.

$$k_z = \frac{\omega}{c_0}\sqrt{\frac{\varepsilon_{r_d}\varepsilon_{r_m}}{\varepsilon_{r_d} + \varepsilon_{r_m}}} \tag{2.10}$$

$$K_m^2 = \left(\frac{\omega}{c_0}\right)^2 \frac{-\varepsilon_{r_m}{}^2}{\left(\varepsilon_{r_d} + \varepsilon_{r_m}\right)} \tag{2.11}$$

To satisfy equation (2.9), $\boldsymbol{\varepsilon_{r_m}}$should be negative. Using Drude model, shown in equation (2.2):

$$\varepsilon_{r_m} < 0 \Rightarrow \omega < \omega_p \tag{2.12}$$

On the other hand, looking at equation (2.11), k_z should be real to have propagating mode in z direction. Since the numerator in square root is negative, so denominator should be negative too.

$$\boldsymbol{\varepsilon_{r_m} + \varepsilon_{r_d} < 0 \Rightarrow \omega < \frac{\omega_p}{\sqrt{1+\varepsilon_{r_d}}}} \tag{2.13}$$

This means that by increasing the dielectric constant of medium above the metal, the cutoff frequency for plasmonic wave will be decreased as is shown in Fig. 2.2.

$$k_z^2 = \frac{\varepsilon_{r_d}\omega^2\left(\omega^2 - \omega_p^2\right)}{c_0^2\left(\omega^2\left(1+\varepsilon_{r_d}\right) - \omega_p^2\right)} \tag{2.14}$$

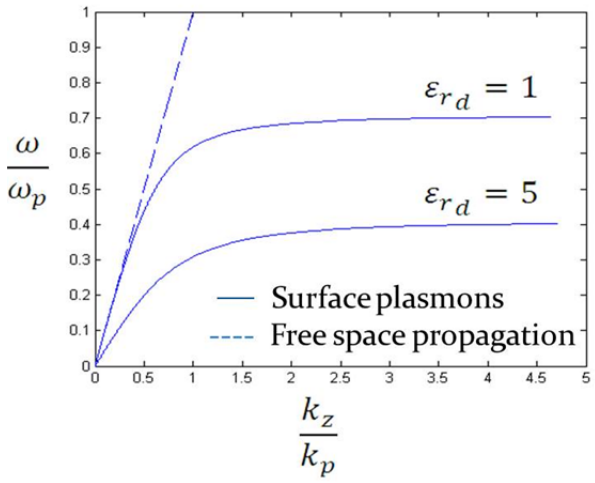

Figure 2.2 Dispersion diagram of surface plasmon wave for two different dielectrics, $k_p = \frac{\omega_p}{c_0}$

As can be seen from Fig. 2.2, the propagation constant of plasmonic waves are on the right side of the free space wave number. This means that these waves cannot be excited by free space propagating waves and specific techniques should be used for the excitation of these waves. There are different methods for excitation of surface plasmon waves which will be discussed in section 2.1.2. It should be noted that if damping be included in the Drude model, then surface plasmon mode will be bounded to a maximum value [9].

In plasmonic wave, field components are decaying exponentially in both dielectric and metal mediums and the mode is confined to the interface. Decaying constant for dielectric medium is defined as K_d. Using this parameter, the confinement factor, which shows how much is the field confined to the metal surface, can be defined as:

$$L = \frac{1}{|Im(K_d)|} \tag{2.15}$$

This definition for the confinement factor means that by the length of L away from metal surface, field amplitude will be decayed by the factor of *1/e*. Using silver and gold

parameters as examples, following confinement factor can be calculated at operating wavelength equal to 600 nm:

Silver: $L = 390\ nm$

Gold: $L = 280\ nm$

This calculations show that there is sub-wavelength confinement in both cases, and gold has more confinement than silver at this wavelength.

The confinement property of plasmonic waves is one of its important properties which make it useful for sensing and imaging of sub-wavelength samples.

2.1.2 Surface Plasmon Excitation

Fig. 2.2 shows dispersion diagram of TM mode for two cases of dielectric permittivity. Both lines are on the right side of free space propagation line, which means that the propagation constant is greater than the wave vector in the dielectric leading to evanescent decay on both sides of the interface. So excitation by free space beams is not possible unless specific techniques for phase-matching are used [9]. There are different methods for surface plasmon excitation: prism coupling, grating coupling, excitation using highly focused optical beams and some other method.

Prism coupling

This method is one of the easy and well established methods and is shown in Fig. 2.3.

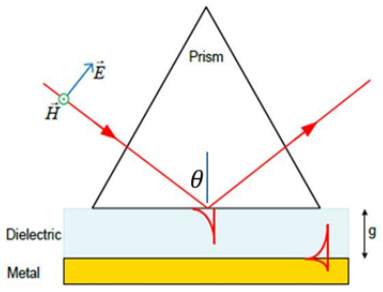

Figure 2.3 Surface plasmon excitation using prism

In this method a dielectric layer exist between prism and metal as shown in Fig. 2.3. The light is shining at the interface of prism and dielectric layer from inside of prism. For incident angles greater than critical angle, total internal reflection will happen at the prism and dielectric layer interface and the light will be reflected. Total internal reflection will create evanescent waves in the dielectric layer. Because the wave in the dielectric layer is evanescent so its propagation constant along the interface is greater than wave number in the dielectric, which means that surface plasmon polaritons can be excited by this evanescent field. When phase constant of light becomes equal to the phase constant of the surface plasmon polariton mode, then light will be coupled to the surface plasmon polartiton mode. Phase matching condition is:

$$k_z^{sp} = n_p k_0 \sin(\theta) \tag{2.16}$$

This phase matching condition happens at a certain incident angle. When light is coupled to the surface plasmon polariton mode, the reflected wave will become small. So by scanning incident angle and looking at the reflection, coupling angle can be measured. The coupling angle is sensitive to the permittivity of the dielectric medium near the surface of the metal. This mechanism has been used to measure refractive index of a sample with high accuracy in the order of 10^{-7}.

Grating Coupling

The mismatch between plasmonic propagation constant and free space wavenumber can also be overcome by patterning the metal surface with a shallow grating of grooves or holes [9]. As the simple case, one dimensional grating is shown in 2.4 with period of *a.*

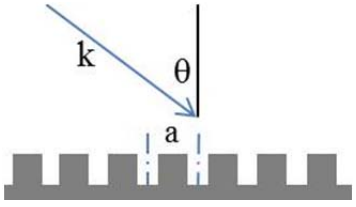

Fig. 2.4 Phase matching of incident beam to surface plasmons polaritons using grating

The phase matching will occur when the relation (2.17) is fulfilled in which $g = \frac{2\pi}{a}$ and $v = 1, 2, \ldots$

$$\beta = ksin(\theta) \pm vg \tag{2.17}$$

Like prism coupling, coupling to surface plasmon polaritons is detected when a minimum occur in the reflected light.

2.2 THz Plasmonics

Many important chemical and biological molecules have their vibrational and rotational resonance frequencies in the THz range that makes the sensing one of the most important applications of THz range. Highly sensitive sensors and high resolution imaging systems are needed in THz range of frequency. High confinement and large field enhancement at surface in surface plasmon polariton waves make it a good option for sensing and imaging applications.

The difference between THz and optical surface plasmon stems from different permittivity at these frequencies. The plasma frequency for many metals falls in the visible and ultraviolet part of spectrum as can be seen for several metals in table 2.1.

Metal	f_p [THz]	f_t [THz]
Al	3570	19.80
Co	960	8.85
Cu	1788	2.20
Au	2184	6.45

Table 2.1 frequency constants for some metals

These characteristic frequencies result in large permittivity of metals at THz frequencies. For example, for gold at 1 THz, relative permittivity will be $\varepsilon_m = -1.22 \times 10^5 - j7.24 \times 10^5$. Using the definition for confinement factor in equation (2.15):

$$\text{Gold: } f = 1\,THz,\ \lambda = 300\,\mu m, L = 2.7\,cm = 89.7\,\lambda$$

As can be seen, there is no sub-wavelength confinement for surface plasmon waves at THz frequencies.

A candidate for guiding confined surface waves at THz frequencies is a periodically structured metal. It has been shown that surface waves on different types of properly designed periodic metallic structures have behavior very similar to plasmonic wave in optical range [2].

Fig. 2.5 shows some periodic metallic structures that can support surface waves.

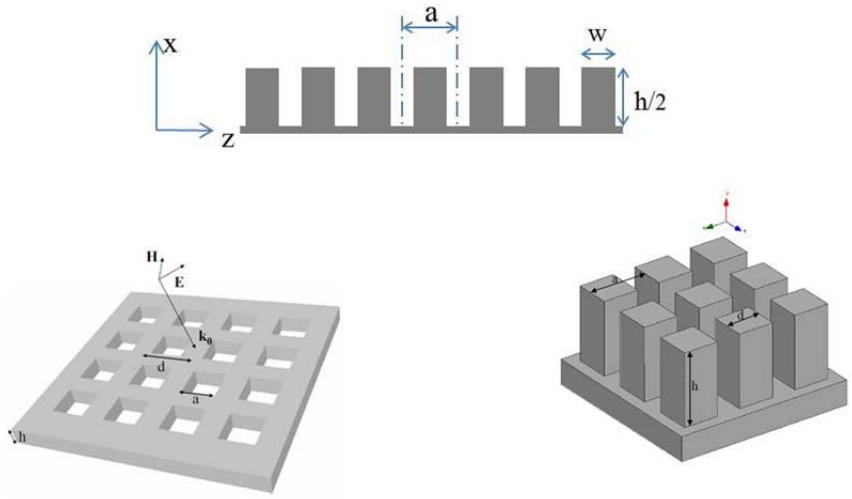

Figure 2.5 some periodic metallic structures which can support surface waves

First one is one dimensional metallic grating and the next one is two dimensional array of holes in metal film. These two structures can be analyzed by analytic methods with some

assumptions and will be presented in the rest of this chapter. The last structure, which is a two dimensional array of metallic rods on a metallic plate will be the subject of chapter 3.

First one is one dimensional metallic grating shown in Fig. 2.6. As is proved below, this metallic grating supports a TM_z surface wave propagating in z direction.

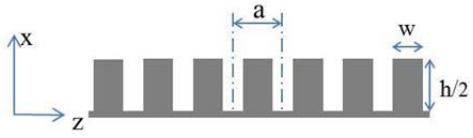

Figure 2.6 One dimensional metallic grating which supports surface waves

To have a simple analytic method, when the dimensions are very smaller than the wavelength, these gratings can be approximated as short circuit parallel plate waveguides [10]. We can suppose general form of a TM_z field distribution for the region above grating, ($x \geq h/2$).

For $x \geq h/2$ TM_z mode:

$$\vec{A} = \psi\hat{z} \quad \vec{F} = 0$$

$$\psi = Be^{-vx}e^{-j\beta z} \quad z \geq h/2 \qquad -v^2 + \beta^2 = k_0^2$$

$$E_z = \frac{1}{j\omega\varepsilon_0}\left(\frac{\partial^2}{\partial z^2} + k_0^2\right)\psi = \frac{-v^2}{j\omega\varepsilon_0}\psi$$

$$H_y = -\frac{\partial}{\partial x}\psi = +v\psi$$

$$z_{up} = \frac{E_z}{-H_y} = \frac{1}{j\omega\frac{\varepsilon_0}{v}} = \frac{1}{j\omega C} \quad \text{For } x \geq h/2$$

For $x \leq h/2$ $z_{down} = jz_0 \tan(k_0 h/2)$

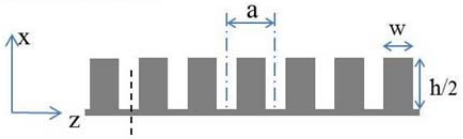

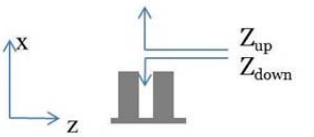

$$z_{up} + z_{down} = 0$$

If the distance between two adjacent gratings is much smaller than the wavelength, then it can be approximated as a parallel plate waveguide which has TEM waves, so transmission lines formulas can be used. z_{down} is calculated based on the formula for short circuit transmission line.

The condition of $z_{up} + z_{down} = 0$ is called transverse resonance condition. This method ends up with dispersion relation of [10]:

$$\frac{-j}{\omega\frac{\varepsilon_0}{v}} + jz_0 \tan(k_0 h/2) = 0 \tag{2.18}$$

Because the first term in equation (2.18) is negative, it can be satisfied only when the second term is positive. This means that it can be satisfied only for $\frac{h}{2} \leq \frac{\lambda}{4}$. So to have surface wave on a simple metallic grating, the height of gratings should be smaller than half of the wavelength.

Fig. 2.7 shows the dispersion relation from this method and also simulation results from COMSOL software. The difference is because of assumptions used in analytic method. Gratings were assumed to be single mode parallel plate waveguides and then transmission line formula was used.

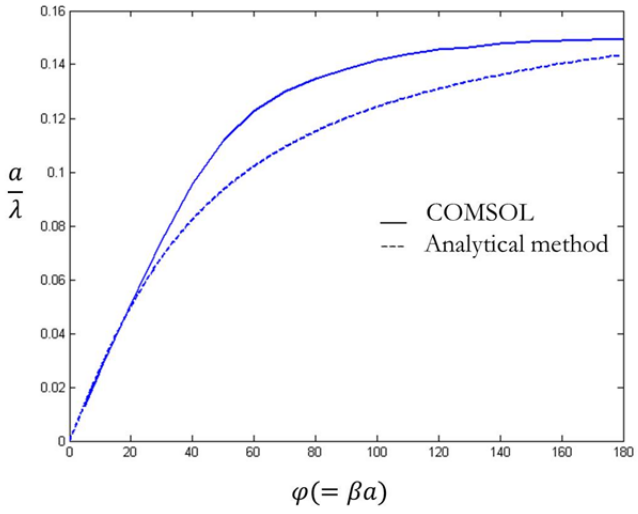

Figure 2.7 Dispersion diagram of surface wave on one dimensional metallic grating derived from analytic formula and COMSOL simulation

Fig 2.8 shows the filed distribution on the structure. It can be seen that fields are confined around the grating. Since grating are smaller than half of the wavelength, so there is sub-wavelength confinement for the fields, like fields of plasmonic waves in optical frequencies.

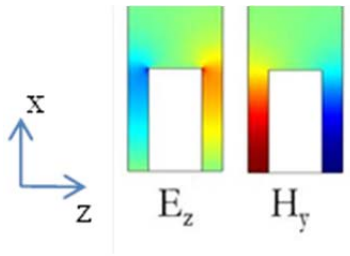

Figure 2.8 Field distributions for surface wave on metallic grating

Figure 2.9 shows the E_x component of electric filed on a line along x axis at the wavelength of 204 μm. As can be seen, the field is confined in around 60 μm region which is sub-wavelength.

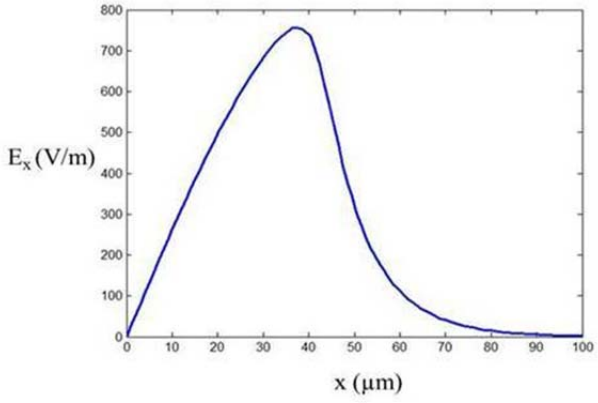

Figure 2.9 E_x component distribution on a line along x axis

As another structure, which is discussed here to show the similarity of surface waves in periodic metallic structures to plasmonic waves at optical frequencies, is a two dimensional array of holes in a metallic plate, shown in Fig. 2.10.

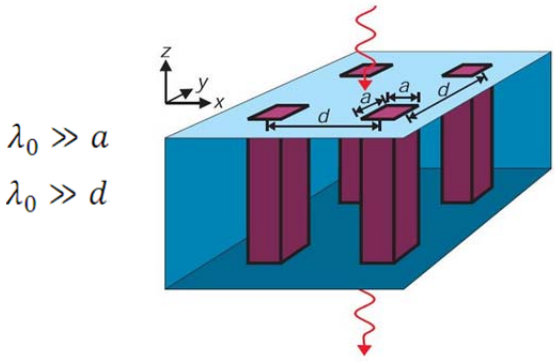

Figure 2.10 Two dimensional array of holes in a metallic film

This structure, also like previous case, can be analyzed by analytical method with assumptions that holes dimensions and the periodicity of the structure are much smaller than the wavelength. In [11] an analytical method has been presented to model this structure by a homogenous layer which has frequency dependent permittivity and find the permittivity which is shown in equation (2.19) here:

$$\varepsilon = \frac{\pi^2 d^2 \varepsilon_h}{8a^2}\left(1 - \frac{\pi^2 c_0^2}{a^2 \omega^2 \varepsilon_h \mu_h}\right) \quad \leftrightarrow \quad \omega_p = \frac{\pi c_0}{a\sqrt{\varepsilon_h \mu_h}} \tag{2.19}$$

This relation from [11], contain physical parameters of the structure which are shown in Fig. 2.10, the parameters of material inside holes, ε_h and μ_h. The form of this relation based on dependency to frequency, ω, is very similar to the Drude model for metals at optical frequencies. This shows the similarities between periodic metallic structures at low THz frequency to the metals at optical range.

Chapter 3

THz Sensing by Plasmonic-like Waves

In the chapter 2 palsmonic-like waves on some periodic metallic structures was discussed and the similarity to optical plasmonic waves was presented. Many groups have used periodic metallic structures with plasmonic-like waves for THz applications. In this chapter, first we present some of these works then a two dimensional array of rods will be discussed as THz refractive index senor.

In [12] a two dimensional array of holes in a metal film is used as a terahertz surface plasmon imaging system. The structure is illuminated with THz wave and transmission is measured. It is shown in [12] that there is a peak in transmittance which is dependent on the dimension of the structure. Fig. 3.1 shows the magnitude of E_z component near the structure.

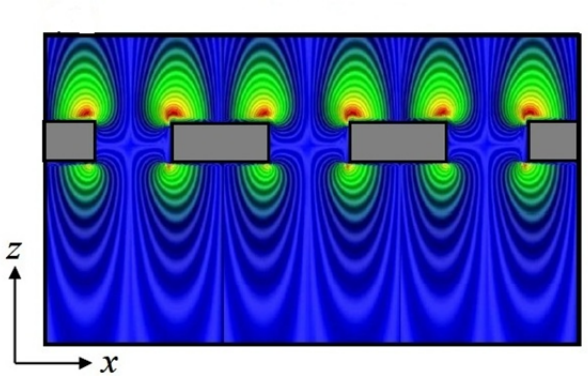

Fig. 3.1 E_z distribution near the structure [12]

Because of the confinement of fields, the structure is sensitive to the medium around the structure so it can be a sensitive sensor [12].

In [13] a fiber based plasmonic sensor for THz range is presented using Polyvinylidene fluoride (PVDF). Dielectric constant of PVDF has negative real part and by analogy with the metal in optical range, PVDF should be able to support plasmonic wave in THz regime [13].

Fig. 3.2 shows the structure. The photonic crystal based core carry the wave and PVDF is positioned on the cladding of fiber. When phase matching is satisfied, coupling to SPP will occur and transmission through the fiber shows a minimum in this case [13].

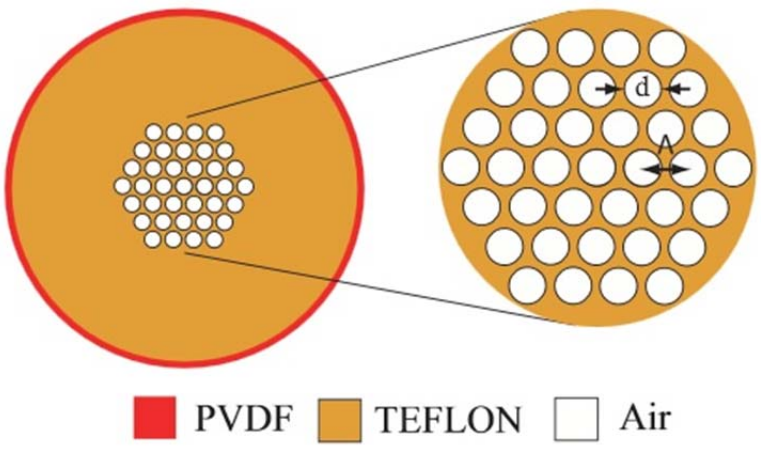

Fig. 3.2 Schematic of THz fiber based sensor presented in [13]

Figure 3.3 shows field distribution in structure when SPP is not excited (a) and when SPP is excited (b) [13].

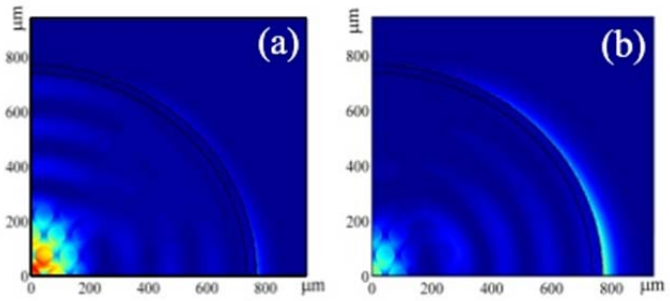

Fig. 3.3 (a) phase match is not satisfied and wave is not coupled to the SPP (b) phase match condition is satisfied and wave is coupled to the SPP

In the rest of this chapter, another metallic structure, which was introduced in [8], is considered. Simulations on sensitivity of the structure to a thin sample and simulations on performance degradation due to fabrication errors are added to previous work.

Fig. 3.4 shows the structure. This structure is not as simple as structures considered in previous chapter and so analytical method cannot be used to analyze it. HFSS simulations can be used to analyze this structure. Then based on the surface waves in this structure, THz refractive index sensor with prism excitation scheme will be discussed. The structure is a two dimensional array of metallic rods on a metallic plate. The height of columns is h = 60 μm and periodicity is a = 50 μm and columns thickness is d = 30 μm.

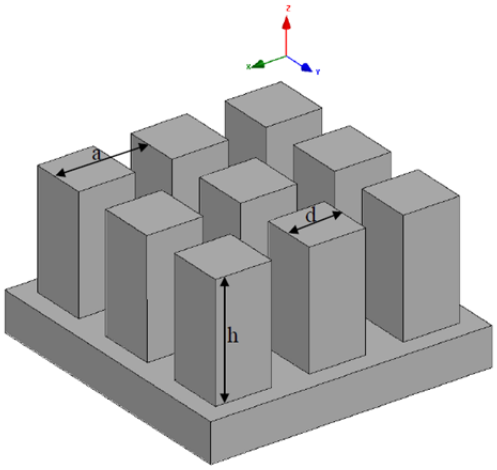

Figure 3.4 Two dimensional array of metallic rods on a metallic plate [8]

3.1 Analysis of the Structure

For the analysis of the structure HFSS software has been used. As shown in Fig. 3.5, just one unit cell of the structure is sufficient to be considered. On top of the unit cell a Perfect Matched Layer (PML) has been put to absorb the waves. In order to find the band-diagram of this photonic crystal, periodic boundary condition mode of HFSS is used.

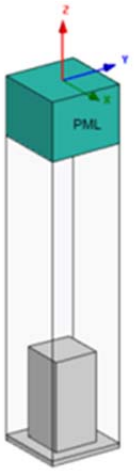

Figure 3.5 One unit cell of the structure in HFSS [8]

In plane components of wave vector, k_x and k_y, generate phase difference between sidewalls of each unit cell. Phase difference between to sidewalls with normal vector in x direction will be shown by $\boldsymbol{\phi_x}$ and for the sidewalls with normal vector along y will be shown by $\boldsymbol{\phi_y}$ as shown in Fig. 3.6. If the periodicity in both x and y direction is equal to a, like our case, then $\boldsymbol{\phi_x = k_x a}$, $\boldsymbol{\phi_y = k_y a}$. For each specific value of $\boldsymbol{\phi_x}$ and $\boldsymbol{\phi_y}$, the eigen-frequency solver of HFSS should be run to find the frequency related to that specific phase differences. In this way band-diagram of photonic crystal is constructed point by point.

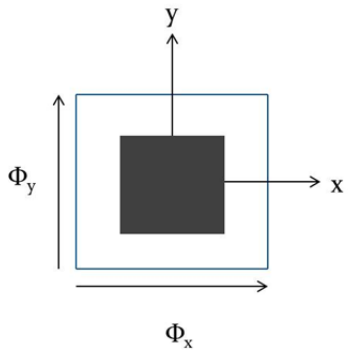

Figure 3.6 Top view of unit cell showing phase differences between sidewalls

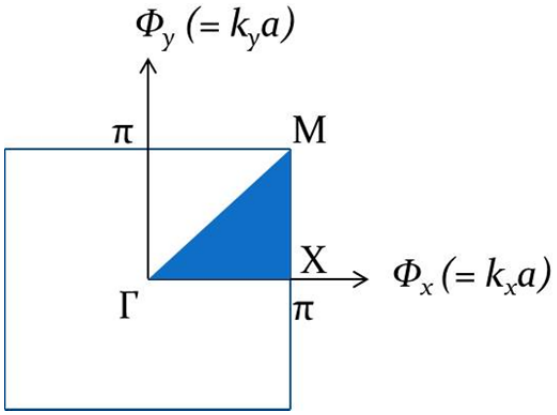

Figure 3.7 Plane of Φ_x and Φ_y,

Fig. 3.7 shows the plane of $\boldsymbol{\phi_x}$ and $\boldsymbol{\phi_y}$. Because of symmetry, it is sufficient to consider just the triangle which is shown in this figure. By changing ($\boldsymbol{\phi_x}$, $\boldsymbol{\phi_y}$) from point Γ to X and then to the point M and again to the point Γ, band diagram will be constructed point by point. Figure 3.8 shows the dispersion diagram for the first and second modes of the structure. Horizontal axis shows the phase difference between to boundaries in three sections and the vertical axis presents the normalized eigen frequency. As can be seen there is a band gap between these two modes. In the first mode, the section around X is flat which as is discussed in [8] is desirable for sensing applications.

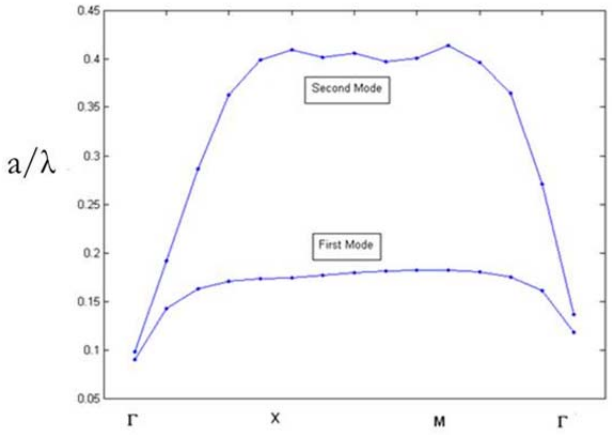

Figure 3.8 dispersion diagram of first two modes of structure presented in [8]

Fig. 3.9 shows the distribution of electric field's magnitude in the first mode at the X point of dispersion diagram. As can be seen, the field is highly confined on the corners of metallic rod like optical plasmonic waves.

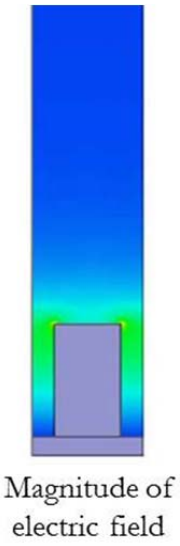

Figure 3.9 Magnitude of electric field is shown in unit cell

The surface wave in this structure is decaying in the medium above the structure and so has propagation constant larger than free space wave number. So like optical plasmonic waves, specific techniques should be used for excitation. Prism is used as coupling scheme [8].

3.2 Surface Wave Excitation Using Prism

Similar to the plasmonic waves at optical frequencies, surface wave on periodic metallic structures has propagation constant greater than the free space wave number, so some techniques should be used for the excitation. One of the well-known methods is using a prism as a coupler. As shown in Fig. 3.10, when phase matching condition is satisfied between the wave inside the prism and surface wave of structure, the wave will be coupled to the surface wave through evanescent waves.

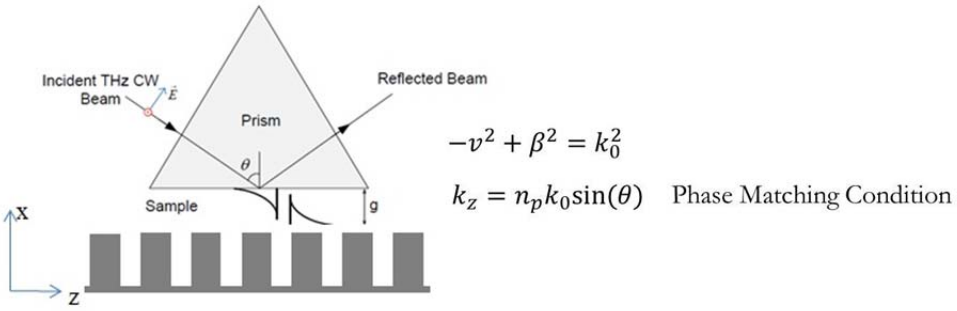

Figure 3.10 Prism coupling to the surface wave of metallic periodic structure

We use a silicon prism with refractive index of 3.42 and base angles of 50 degrees. Looking at the reflected power versus incident angle, at the matching angle, a dip will be observed at a specific angle which is called coupling angle θ_c, Fig. 3.11. At the coupling angle the incident power is coupled to the surface wave and will not be reflected.

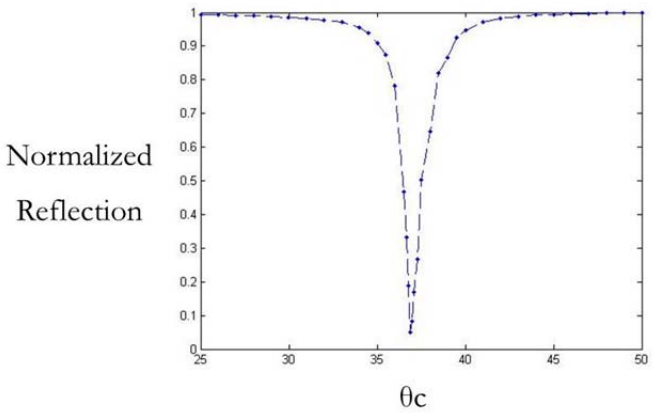

Figure 3.11 Reflection versus incident angle of structure shown in Fig. 3.4

This coupling angle is sensitive to the refractive index of the medium between prism and structure. So coupling angle can be used for refractive index sensing. The sample should be placed between prism and structure at where, the fields are maximum and there will be maximum interaction between field and sample [8].

3.3 Sensitivity and Performance Degradation Due to Fabrication Tolerance

Sensitivity

As discussed in the last paragraph of previous part, the sharp dip in Fig. 3.11 can be used for sensing applications. By measuring the reflection and finding changes in coupling angle, changes in the refractive index of the medium can be measured. In order to analyze the sensitivity of this sensor, a dielectric layer should be placed on top of the structure as the sample. Fig. 3.12 shows the unit cell of structure in HFSS. Because the prism is much larger than the wavelength (base of the prism is a rectangle of 3 cm by 4 cm and height is 3 cm and wavelength is 300 μm), the prism can be assumed as an infinite medium above the structure. The upper cubic in Fig. 3.12 shows the prism. By putting perfect match layer (PML) on top of the unit cell, it can be truncated. The thickness of the sample should be large enough to interact with the whole region of electric field distribution to have the maximum sensitivity. The magnitude of electric field was shown in 3.9. The columns height is 60μm. The thickness is chosen to be 10μm which is λ/30 for 1 THz frequency.

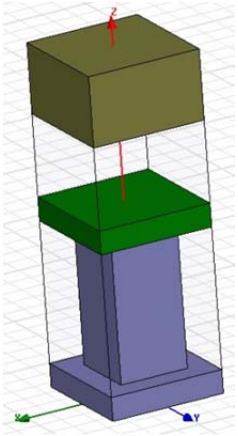

Figure 3.12 Unit cell of structure with dielectric and prism in HFSS (PML is not shown)

Fig. 3.13 shows the coupling angle as a function of dielectric permittivity. This figure shows that when the permittivity of medium changes from 1 to 1.3, the coupling angle will change from 37 degrees to 67 degrees. The minimum sensitivity of the sensor occurs at

permittivity around 1, wherein 0.01 changes in permittivity will cause 0.3º degree change in the coupling angle [14]. If the coupling angle could be measured with the accuracy of 0.01 º, then the sensitivity would be around3×10^{-4}.

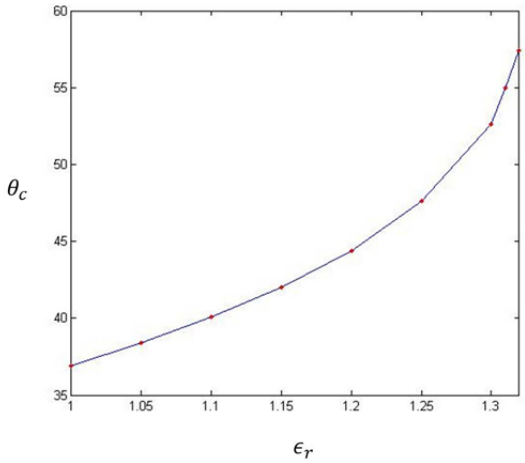

Figure 3.13 Coupling angle as a function of sample dielectric permittivity. Dot points are HFSS results

Performance Degradation Due to Fabrication Tolerance

Strong confinement of the surface plasmonic-like modes in the periodic metallic structures makes the performance of these devices very sensitive to the fabrication errors. One of the parameters, which can be impacted by fabrication error, is the height of columns. HFSS has been used to analyze the effect of fabrication tolerance on the device performance.

Figure 3.14 shows the reflection plot for 3 different column heights of structure in Fig. 3.4, (tolerance of 1 μm).

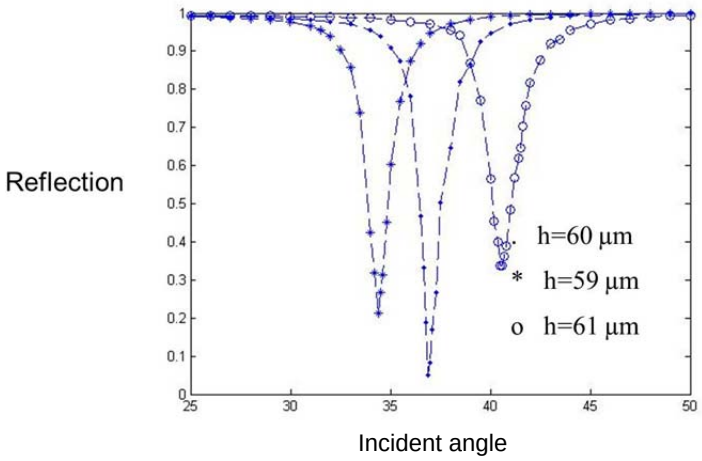

Figure 3.14 Reflection versus incident angle for three different heights of columns

For longer (61 μm) or shorter (59 μm) columns the coupling efficiency will be lost, so in order to have sensitive sensor the fabrication tolerance on the height of columns should be less than 1 μm. Also the coupling angle is changing in a wide range for different heights. This again shows that this device is very sensitive to fabrication errors and this is not good from the practical point of view.

Disadvantages of this sensor:

The sensor which was presented in [8], has been analyzed to find out its sensitivity and fabrication error tolerance in this chapter. Simulations show that the structure performance is very sensitive to the fabrication errors and it need very precise fabrication method. Also, prism coupling scheme which is considered for the excitation, is too bulky. Always there is huge interest in the integrated components, but prism coupling scheme will not allow for integration of this structure.

In recent years, there has been interest on the integrated sensors in optical range which work based on plasmonic waves. In the next chapter an overview of some of these publications is presented. Then an integrated structure for THz sensing based on plasmonic-like waves is presented and simulation results are discussed.

Chapter 4

Integrated THz Plasmonic-like Sensor

Many existing plasmonic or plasmonic-like sensing configurations use prism for plasmonic wave excitation [15]. However prism is too bulky for integration. Interests in integrated surface plasmonic devices at optical frequencies have been growing recently [16, 17]. As compared with free space configuration, integrated structures have distinct advantages such as small size and multi-channel sensing capabilities.

One of the main issues in the integrated plasmonic structures at optical frequencies is coupling between plasmonics mode and other waveguides modes because there is a huge mode mismatch between the mode of a dielectric waveguide and surface plasmon mode at the interface of a metal and a dielectric. We use a metallic grating as THz waveguide with surface plasmon-like mode. As it was discussed in chapter 2, the height of the grating waveguide should be comparable with wavelength in order to support surface wave [17]. The height of a slab waveguide is also roughly in the same order as the metallic grating. Because of the comparable height and also modal similarity between slab waveguide and metallic grating, the mode mismatch is not as large as optical plasmonic mode mismatch. Also it has been shown that a metallic grating can be modeled with an effective slab waveguide [18] which means that with properly designed metallic grating, it will have an effective refractive index equal to the refractive index of slab waveguide. These facts mean that metallic grating can be effectively excited using slab waveguide in longitudinal form to have an integrated component which we present and analyze this idea in this chapter.

First, some recent structures on integrated plasmonic sensing at optical frequency are discussed. Then the grating structure for THz sensing is presented and analyzed.

4.1 Optical Integrated Plasmonic Sensor

In [19] the structure shown in Fig. 4.1 is presented. The Au films on top of a silicon dielectric waveguide, act as plasmonic waveguide. Input and output of the dielectric waveguide are the input and output of the whole structure.

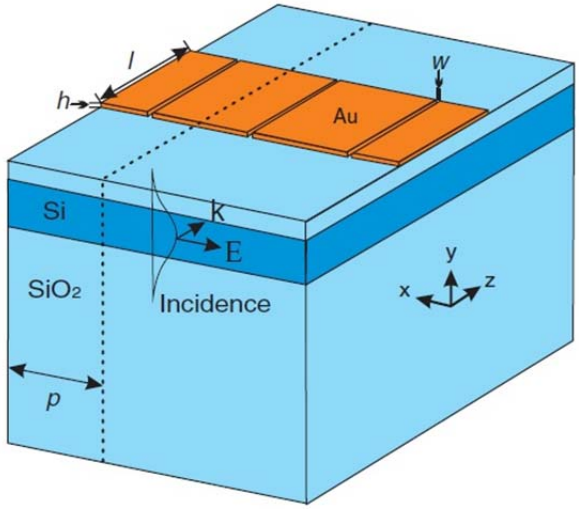

Figure 4.1 Integrated plasmonic optical sensor presented in [19]

The dielectric waveguide mode can be coupled to the plasminc waveguide when phase matching between the dielectric waveguide mode and the plasmonic waveguide mode is satisfied. Fig. 4.2 shows the transmission through dielectric waveguide. The dips show the coupling to surface wave on plasmonic waveguide.

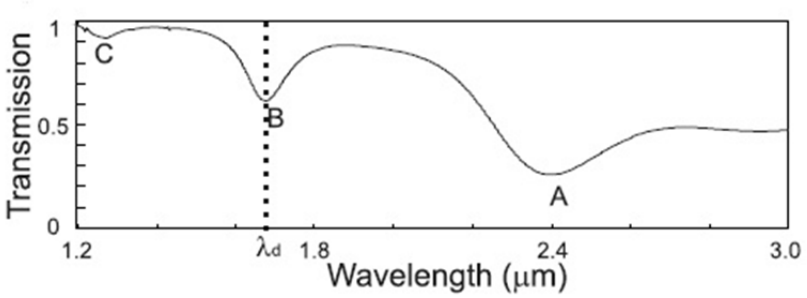

Figure 4.2 Normalized transmission through dielectric waveguide [19]

If we put a sample on top of the plasmonic waveguide, it will change the phase matching wavelength, so the structure can be used as a refractive index sensor [19].

Fig. 4.3 shows another integrated optical palsmonic sensor presented in [20]. There is a vertical plasmonic waveguide on top of dielectric waveguide. Part (b) of figure below shows the coupling situation and there will be a dip in transmission through dielectric waveguide.

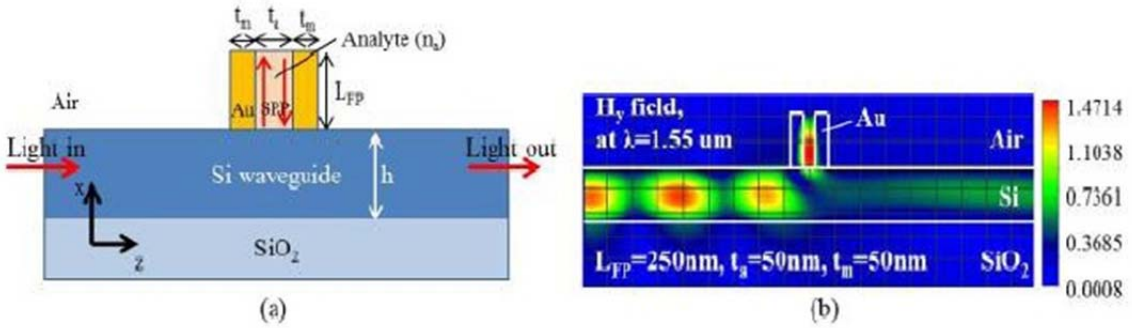

Figure 4.3 Integrated plasmonic optical sensor presented in [20]

It has been presented in [20] that this structure can be used for gas or liquid sensing in configuration shown below.

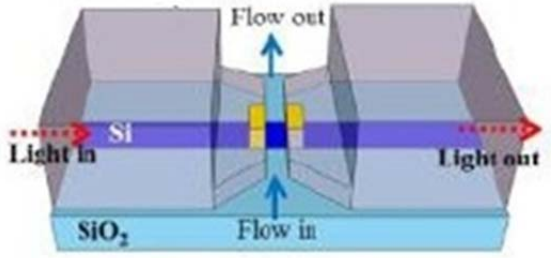

Figure 4.4 Integrated scheme for sensing of liquid or gaseous samples presented in [20]

As can be seen in these examples, it's a very good idea to excite the plasmonic mode using dielectric waveguides which can be integrated with other components like source and detector, which cannot be done when prism is used for excitation. So it would be very interesting to use dielectric waveguide for the excitation of palsmonic-like waves on periodic

metallic structures and then using that to have an integrated sensor. In the rest of this chapter this will be discussed.

4.2 Metallic Grating Waveguide

Fig 4.5 shows metallic grating waveguide which is a uniform grating structure in z direction with grating period of *a*. Metallic rods have rectangular cross section with the width of *w* and height of *h* and. All aforementioned dimensions are in sub-wavelength range. In y-direction, the structure is assumed uniform and infinitely long in the analysis.

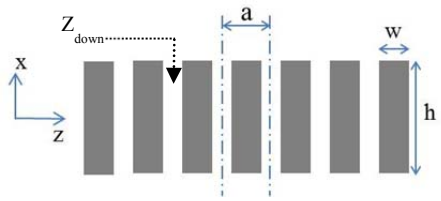

Figure 4.5 Metallic grating waveguide. The structure is uniform and infinitely long along the y-axis.

The fundamental transverse magnetic to *z* (TM_z) mode is considered here. As it is discussed in [18] and discussed in chapter 2 as well, as long as the distance between two adjacent metallic rods is very small as compared with the wavelength, two adjacent rods can be approximately modeled as a parallel plate waveguide with transverse electromagnetic (TEM) field distribution and can be analyze by transmission line theorem. Using transverse resonance method, impedance looking in *x*-direction should be found. Using open circuit transmission line formula, input impedance in Fig. 4.5 can be calculated as:

$$Z_{down} = \frac{E_z}{H_y} = \frac{-jZ_0}{\tan(\beta h)} \tag{4.1}$$

As calculated in page 14, Z_{up} is capacitive impedance. To have a surface wave propagating in *z*-direction $Z_{up} + Z_{down} = 0$ should be satisfied. So Z_{down} should be inductive which using equation (4.1), means that *h* should be between λ/4 and λ/2. Transmission line model, described above, provides an initial design value for the height h. For analysis of the

proposed grating waveguides, we consider one unit cell and use periodic boundary condition along the propagation direction (z-axis) in COMSOL. For a given value of phase difference between the periodic boundary planes, an eigen-value problem is solved resulting in an eigen-frequency and its corresponding modal field. By choosing dimensions as a = 30 μm, w = 17 μm and h = 85 μm, (details on choosing the dimensions is presented in the end of section 4.4) the structure has been analyzed in COMSOL. By changing the phase difference between to sidewalls, dispersion diagram can be generated point by point.

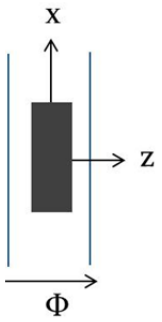

Figure 4.6 One unit cell of grating is sufficient to be considered. COMSOL is used for simulation

Fig. 4.7 shows the dispersion diagram of the first and second plasmonic-like modes for metallic grating waveguide of Fig. 4.5 with perfect electric conductor (PEC) and silver rods.

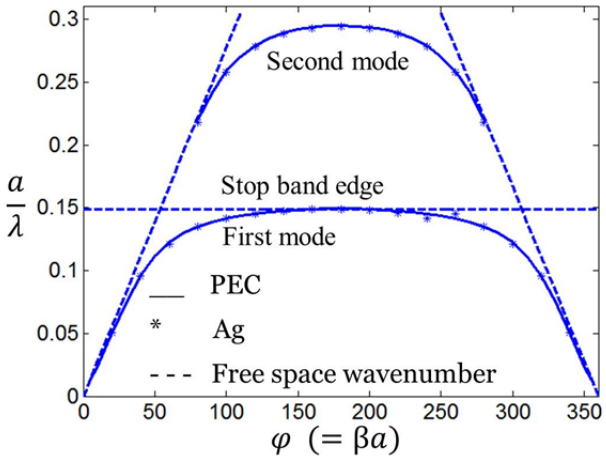

Figure 4.7 Dispersion diagram of the grating waveguide of Fig. 4.5 for the first two plasmonic-like modes for PEC and silver rods.

Plots in Fig. 4.7 for PEC and silver rods are almost identical that supports the fact that the plasmonic-like modes are mostly due to the periodicity and physical dimensions of the metallic structure in THz range and not from the bulk property of the metal as in optical range. From the dispersion diagram in Fig. 4.7, it can be seen that the frequency is increasing for phase difference below $\beta a=180^{\circ}$, and after this point it start to decrease, so there is a maximum allowed frequency and this is the starting point of band gap of the grating. Also, the propagation constant of these modes are greater than free space wave number, so as discussed in chapter 2, specific techniques should be used for excitation. This will be topic of next section.

Fig. 4.8 shows the *x* component of electric field and *y* component of magnetic field, respectively, of the first plasmonic-like mode of grating waveguide.

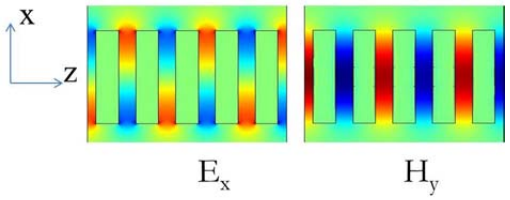

Figure 4.8 Field distribution of the first plasmonic-like mode of metallic grating waveguide at 1.47 THz (λ = 204.1 μm)

As shown in Fig. 4.8, E_x is strongly confined to the surface with sub-wavelength extension in free space. Fig. 4.9 shows the amplitude of E_x component in the range x = 0 -100 μm, in the middle of two adjacent rods. ($x = 0$ is the middle of rods in x direction, structure is symmetric around $x = 0$.) As shown in Fig. 4.9, the field is exponentially decaying above the grating in free space (x > 42.5 μm) with sub-wavelength confinement for frequencies in the pass-band. It should be noted that the advantage of metallic grating versus dielectric grating is that fields are highly confined in metallic grating. The field confinement makes the structure suitable for very sensitive and highly accurate refractive index measurement as will be discussed in the next sections.

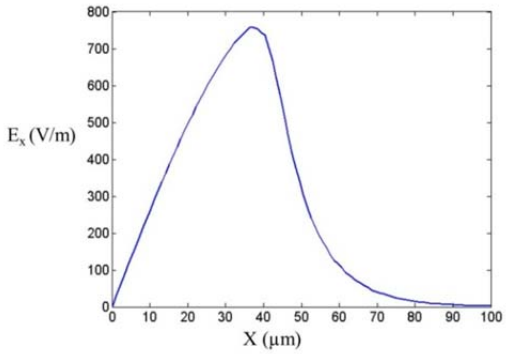

Figure 4.9 Amplitude of E_x in the middle of two adjacent rods versus *x* coordinate, at 1.47 THz (λ = 204.1 μm).

Finding the dispersion diagram, COMSOL gives a complex number as eigen frequency. The imaginary part of this complex number is related to the attenuation factor α:

$$e^{jkz} = e^{j\frac{2\pi f}{c}z} = e^{j\frac{2\pi f_r}{c}z} e^{-\frac{2\pi f_i}{c}z} \tag{4.2}$$

$$\alpha = \frac{2\pi f_i}{c} \tag{4.3}$$

$$Loss\ (dB/mm) = 20 \log e^{-\alpha \times 0.001} \tag{4.4}$$

In Fig.4.10, the calculated loss of the waveguide made of silver has been shown.

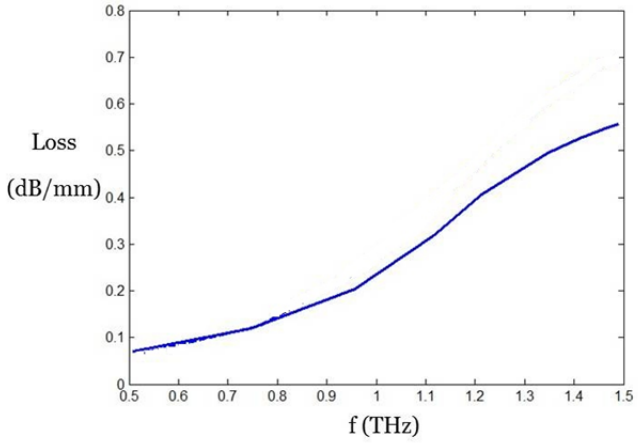

Figure 4.10 Propagation Loss of the first plasmonic-like mode for grating waveguide made of silver.

4.3 Excitation of Metallic Grating Waveguide Using Slab Waveguide

In previous section it was concluded from Fig. 4.7 that the modes of the grating waveguide has propagation constant greater than free space wave number and so cannot be directly excited by free space waves. Excitation of plasmonic and plasmonic-like waves using a prism is well known which was discussed in chapter 2 and was used in chapter 3. But, prism is too bulky for integration and it is desirable to excite plasmonic waves with dielectric waveguides, as discussed in the beginning of this chapter. Because of mode mismatch between plasmonic mode and dielectric waveguide, efficient coupling between them is difficult although is not impossible [19-21]. But for plasmonic-like modes in periodic metallic structures, the situation is different. As discussed and numerically shown in previous section, to have surface wave in a one dimensional metallic grating, the height should be greater than a quarter of wavelength which is comparable with the height of a slab waveguide. Fig. 4.11 shows E_x and H_y field distributions of the first TM mode of a dielectric slab waveguide.

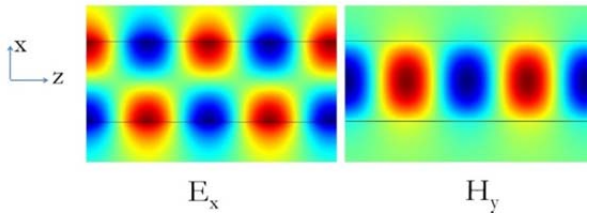

Figure 4.11 E_x and H_y field distribution of first TM mode in a dielectric slab waveguide.

By comparing the field distributions in Fig. 4.11 with that in Fig. 4.8, clear similarities can be seen between the first plasmonic-like mode of the metallic grating waveguide and the first TM mode in a dielectric slab waveguide. Both have peak of *x*-component of electric field at two ends with odd symmetry and also both have the peak of magnetic field in the middle (x = 0). As shown in Fig. 4.9, fields of grating are exponentially decaying above the grating which there is the same form for evanescent field in the cladding region of slab waveguide. So such

observation may suggest that the grating waveguide can be effectively excited by slab waveguide in longitudinal form, Fig. 4.12.

Figure 4.12 Longitudinal excitation of a metallic grating by slab waveguide

To have an efficient coupling between slab waveguide and metallic grating waveguide, first, they should have the same height in order to have overlap between the peaks of electric field of grating and slab waveguides, and for magnetic fields as well. An effective slab model for metallic grating is presented in [18]:

$$n_{eff} = \frac{a}{a-w} \tag{4.5}$$

In which, *a* is periodicity of grating and *w* is the width of each column (*w* is like a filling factor of periodic structure). So choosing the same height for slab and grating waveguides will maximize the field peaks overlap, and properly choosing *a* and *w*, will minimize the refractive index mismatch.

The structure shown in Fig. 4.12 has been analyzed using full wave simulation of COMSOL and Fig. 4.13 shows the transmission and reflection spectrum of the structure.

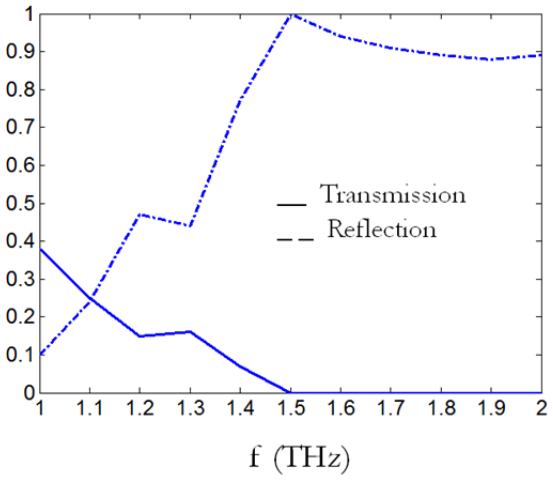

Figure 4.13 Transmission and reflection spectrum of the structures shown in Fig. 12

As can be seen in Fig. 4.13, there is a cut-off for transmission around 1.495 THz and the transition between pass-band and stop-band is gradual. In the next section we will discuss using this structure as a sensor. A sharp transition between pass-band and stop-band will increase the sensitivity of the sensor.

In Fig. 4.12 it can be seen that the structure is a cascading of three waveguides. The gradual transition to the band gap in Fig. 4.13 means that there is not good matching between dielectric waveguide and grating before cut off frequency, this can be because of the modal shape of two waveguides which are not exactly the same. Maybe having a tapering transition between waveguides will give a better matching which will conclude in a sharp transition to band gap.

Fig. 4.14 shows the structure with tapering sections between grating and slab waveguides. The goal is to have maximum transmission through structure before the band gap frequency of the grating. To make the structure smaller, the minimum tapering section is desirable. Tapering section can be around the wavelength to have good matching between waveguide. As will be discussed on next section we want to use this structure in the band width of 1.1 THz to 1.5 THz as a sensor for which wavelength is between 200 μm to 270 μm. Using full wave simulation in COMSOL, tapering with the length of 240 μ which for periodicity of 30 μm is equal to 8 tapered cells is used [22].

Figure 4.14 Excitation of a metallic grating by a slab waveguide with tapering

Fig. 4.15 shows the transmission and reflection spectrum of the structure shown in Fig. 4.14 [22].

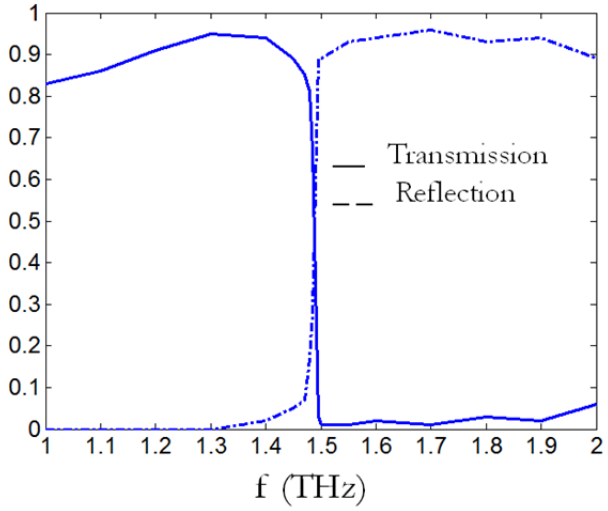

Figure 4.15 Transmission and reflection spectrum of the structures shown in Fig.14

As can be seen in Fig. 4.15, there is a cutoff at 1.495 THz again like Fig. 4.13, but the transition is very sharp in this case. The reason for this sharpness is that, because of good matching between dielectric waveguide and grating, there is around 90% transmission before the band gap frequency, and when it reaches the band gap frequency it will be suddenly fall down because the grating structure will not allow any transmission after the band gap frequency; and these two phenomena together, make a sharp transition in transmission and reflection spectrums.

The sharp transition edge makes the structure of Fig. 4.13 suitable for refractive index sensing. Fig. 4.16 shows the field distribution of H_y component for two frequencies below and above the transition edge frequency, using COMSOL simulations. A high transmission is evident in Fig. 4.16 at 1.485 THz that is slightly below the transition frequency (1.495 THz) whereas almost no transmission occurs at 1.500 THz that is slightly above the transition frequency.

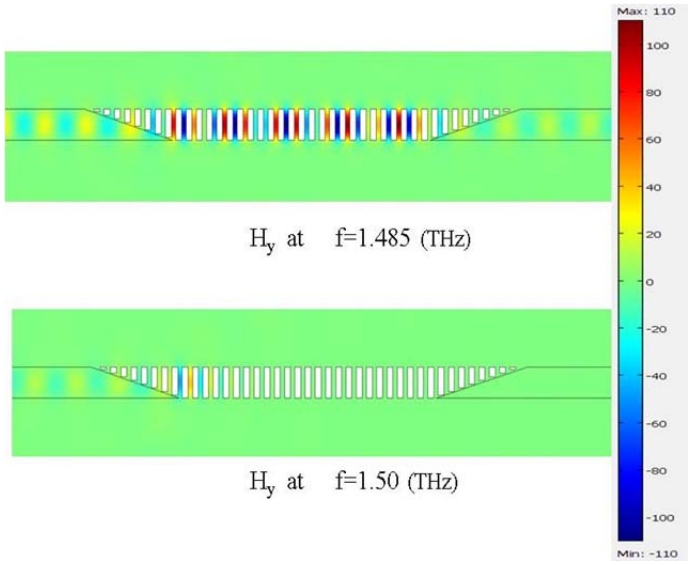

Figure 4.16 H_y distribution for frequencies below (top) and above (bottom) of the transition edge frequency

4.4 Sensitivity of the Proposed Structure

The transition edge frequency of grating varies sensitively when the refractive index of the surrounding medium changes. Because of highly confined field around the metallic grating over sub-wavelength, the structure is highly sensitive to the small changes in refractive index of the sample. Fig. 4.16 shows the sensitivity of the transition edge frequency with respect to the refractive index of in the range of n = 1-1.44. The sample covers all around the grating.

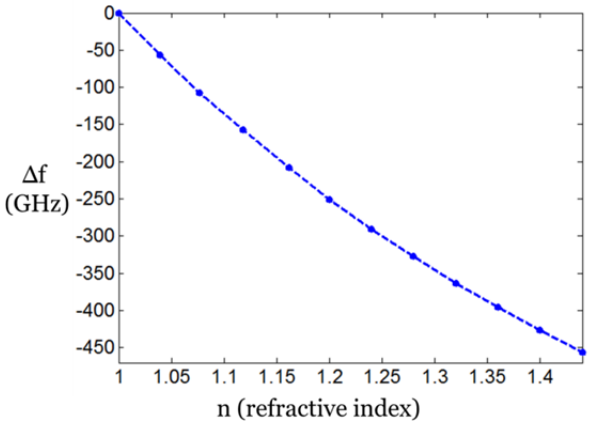

Figure 4.17 Sensitivity of the stop-band edge frequency of the grating to the refractive index of the surrounding medium.

Using results shown in Fig. 4.16, the sensitivity is around 1480 GHz/RIU (Refractive Index Unit) for small refractive indices around 1, and it decrease to 733 GHz/RIU for refractive indices around 1.44. Using a system with 30 MHz resolution, the sensitivity is 2×10^{-5} for refractive indices around 1, and is around 1×10^{-5} for indices around 1.44. This is one order of magnitude more sensitive than the structure discussed in chapter 3.

As a comparison with other works, [13] presents a fiber based integrated THz sensor which its mechanism was briefly discussed in the beginning of chapter 3 as well. It reports sensitivity of 10^{-4} for gaseous analyte samples.

Reference [23] presents an integrated parallel plate waveguide based sensor for refractive index sensing and reports 10^{-3} resolution in refractive index.

Choosing the dimensions of Grating:

The designed grating is excited with dielectric slab waveguide. In the sensing application of the structure, as Fig. 4.17 shows, the stop-band edge frequency is decreasing by increasing the refractive index of sample, for the sample with refractive index of 1.4, stop-band edge will decrease from 1.495 THz to 1.1 THz. So it is important to have efficient coupling between slab and grating waveguides for a frequency band of 1.495 THz to 1.1 THz.

As can be seen from Fig. 4.15, before the stop-band edge, the transmission will increase by increasing the frequency. This is due to the fact that at higher frequencies, the taper's length is longer in terms of wavelength and it will have better matching. So propagation constant should be matched for worst case of coupling which is the lowest frequency of desirable band, 1.1 THz. By properly choosing the dimensions of grating, as is discussed below, propagation constant for grating and slab has been matched at 1.1 THz, using COMSOL for simulations. For slab waveguide, Silica with refractive index of n = 1.96 has been used [24].

The periodicity, *a*, mainly determines the band gap frequency. To have band gap around 1.5 THz, a = 30 μm, is chosen. The goal is to have the same propagation constant in grating

and slab waveguide at 1.1 THz, because in this way, the decaying factor of the fields above both waveguide would be the same. This will result in better matching in the field profile of waveguides and so higher transmission. Using COMSOL simulation for each value of *w* (width of rods), frequency related to the desired propagation constant can be found. The value of *w* is adjusted in order to make this frequency equal to 1.1 THz. The result is $w = 17$ μm.

Technical difficulties of proposed sensor

Good dielectric waveguide in THz range is still a challenge. Also the mechanism for coupling into the dielectric waveguide is another issue. Here we have just assumed a simple slab waveguide at THz range to proof the concept of sensor structure.

Another issue is fabrication of the grating specially the tapering section. The tapering section can be approximated by several steps to make it easier for fabrication.

As a conclusion of this chapter, excitation of a metallic grating structure using dielectric slab waveguide in a longitudinal structure has been proposed. Periodic metallic structures which support surface palsmon-like waves can be used for different components at THz frequencies. Possibility of excitation of metallic grating using dielectric waveguide allows using the grating in integrated form. Integrated sensing configurations have many advantages such as low cost, small size and the capability for multi-channel sensing for high throughput. Band-stop edge of the metallic grating is sensitive to the refractive index of surrounding medium. Sensitivity of this integrated THz refractive index sensor has been presented.

Chapter 5

Conclusion

Using plasmonic-like waves for Terahertz sensing application was the topic of this thesis. THz range of frequency has found a fast growing number of applications. Specially because of long wavelength at THz frequencies in compare with optical regime, sensors for sub-wave length samples are important components. Plasmonic are well known for sensing applications in optical frequencies mainly because of their highly confined and enhanced fields. At lower frequencies including THz range, plasmonic waves are not confined to the surface like in optical frequencies. Using periodic metallic structures which support surface waves is a candidate to have waves with properties similar to plasmonic wave at optical frequencies.

A two dimensional array of metallic rods on a metallic plate, which was presented in [8], was considered as a THz sensor with prism excitation method. The analysis of structure using HFSS was presented. Here, using HFSS simulations we found that sensitivity of sensor, for accuracy of 0.01º in measuring the coupling angle, is 3×10^{-4}. Using HFSS simulations, we showed that this structure is very sensitive to the fabrication error tolerance. This is because of the high confinement of the surface waves which make the performance sensitive to the dimensions of the structure.

We presented an integrated THz sensor based on plasmonic-like waves chapter 4. Excitation of metallic grating using slab waveguide was presented in this chapter. It was shown that this can be done because of similarity between metallic grating mode and the first mode of a slab waveguide. This method has the advantage of integration also it is not bulky like other configurations like prism coupling. We, theoretically present sensing application of the structure for the liquid or gaseous samples. Sensitivity and field distribution results from COMSOL simulations were discussed. We showed that using this structure, sensitivity of the 10^{-5} order is achievable.

Bibliography

[1] M. Tonouchi, “Cutting-edge Terahertz Technology,” Nature Photonics, vol. 1, pp. 97-105, Feb. 2007

[2] Y. S. Lee, “Principles of terahertz science and technology,” Springer 2008

[3] C. R. Williams et. Al., “Highly confined guiding of terahertz surface plamon poalriton on structured metal surface”, Sensors and Actuators B, vol. 54, no. 1-2, pp. 3-15, Jan. 1999

[4] F. Miyamaru, S. Hayashi, C. Otani, K. Kawase, Y. Ogawa, H. Yoshida and E. Kato, “Terahertz Surface-Wave Resonant Sensor with a Metal Hole Arrat,” Optics Letters, vol. 31, no. 8, pp. 1118-1120, April 2006

[5] F. Miyamaru, M. W. Takeda, T. Suzuki and C. Otami, “Highly sensitive surface plasmon terahertz imaging with planar plasmonic crystal”, Optics Express, vol. 15, no. 22, pp. 14804-14809, Oct. 2007

[6] G. Kumar, S. Pandey, A. Cui and A. Nahata, “Planar Plasmonic Terahertz Waveguide Based on Periodically Corrugated Metal Films,” New Journal f Physics 13 (2011) 033024

[7] M. Tanaka, F. Miyamaru, M. Hango, T. Tanaka, M. Akazawa and E. Sano, “Effect of a thin Dielectric Layer on Terahertz Transmission Characteristics for Metal Hole Arrays,” Optics Letters, vol. 30, no. 10, pp. 1210-1212, May 2005

[8] A. Arbabi, A. Rohani, D. Saeedkia and S. Safani-Naini, “A terahertz metamaterial structure for near-field sensing applications”, Proceeding of 33rd International Conference on Infrared, Millimeter and Terahertz Waves, 2008

[9] S. A. Maier, “Plasmonics: Fundamentals and Applications,” Springer, 2007

[10] R. F. Harrington, "Time Harmonic Electromagnetic Fields,"

[11] J. Pendry, L. Martin-Moreno, and F. Garcia-Vidal, “Mimicking surface plasmons with structured surfaces,” Science, 305:847-848, August 2004

[12] F. Miyamaru, M. W. Takeda, T. Suzuki and C. Otani, “Highly Sensitive Surface Plasmon Terahertz Imaging with Planar Plasmonic Crystals”, Optics Express, vol. 15, no. 22, pp. 14804-14809, Oct. 2007

[13] A. Hassani and M. Skorobogatiy, “Surface Palasmon Resonance-like Integrated Sensor at Terahertz Frequencies for Gaseous Analysts”, Optics Express, vol. 16, no. 25, pp. 20206-20214, Dec. 2008

[14] H. Amarloo, A. Rohani and S. Safavi-Naeini, “Sensitivity and Error Analysis of a Surface Plasmonic Mode Metallic Grating Sensor”, Antenna and Propagation Symposium 2012

[15] J. Homola, S. S. Yee, and G. Gauglitz, “Surface plasmon resonance sensors: review,” Sens. Actuators B 54, pp. 3–15, Sep. 1999

[16] A. Hassani, A. Dupuis and M. Skorobogatiy, “Surface-plasmon-resonance-like fiber based sensor at terahertz frequencies,” J. Opt. Soc. Am. B, vol. 25, no. 10, pp. 1771-1775, Oct. 2008.

[17] M. Navarro-Cia, M.Beruete, S. Agrafiotis, F. Falacone, M. Sorolla and S. A. Maier, “Broadband spoof plasmons and subwavelength electromagnetic energy confinement on ultrathin metafilms,” Optics Express, vol. 17, no. 20, pp. 18184-18195, Sep. 2007

[18] J. T. Shen, P. B. Catrysse and S. Fan, “Mechanism for designing metallic metamaterials with a high refractive index of refraction,” Phys. Rev. Lett., pp. 197401(1-4), May. 2005

[19] Q. Tan, A. Cosentino, M. Roussey and H. P. Herzig. Theoretical and experimental study of a 30 nm metallic slot array, in Journal of the Optical Society of America B-Optical Physics, vol. 28, p. 1711-1715, 2011

[20] D. Lee, H Yim, S. Lee, and B. Hoan, “Tiny surface plasmon resonance sensor integrated on silicon waveguide based on vertical coupling into finite metal-insulator-metal palsmonic waveguide”, Optics Express, vol. 19, no. 21, Oct. 2011

[21] G. Veronis and S. Fan, “Theoretical investigation of compact couplers between dielectric slab waveguides and two dimensional metal-dielectric-metal palsmonic waveguides,” Optics Express, vol. 15, no. 3, pp. 1211-1221, Feb. 2007

[22] H. Amarloo, M. Neshat and S. Safavi-Naeini, “Plasmon-like wave integrated sensing applications,” submitted to Electronic Letters

[23] V. Astley, K. S. Reichel, J. Jones, R. Mendis and D. M. Mittleman, “ Terahertz multichannel microfluidic sensor based on parallel-plate waveguide resonant cavities,” Applied Physics Letters 100, 231108, June 2012

[24] M. Naftaly and R. E. Miles, “Terahertz time domain spectroscopy for material characterization,” Proceeding of IEEE, vol. 95, no. 8, pp. 1658-1665, Aug. 2007